NUKLEONIKA 2002;47(4):163–166

ORIGINAL PAPER

Thermal evolution of solid targets irradiated by pulsed plasma beams

Władysław Szymczyk,
Jerzy Piekoszewski,
Zbigniew Werner,
Witold Szyszko

Abstract Thermal evolution of various targets irradiated with high intensity pulsed ion or plasma beams was determined by computer simulation i.e. by solving numerically one dimensional heat flow equation. The calculations were carried out using the adopted ETLIT computer code (Energy Transport in Laser Irradiated Targets) based on Finite Element Method. The surface temperature, melt depth and liquid duration were computed as a function of pulse energy density, pulse duration, melting temperature and thermal diffusivity of a given material. In particular, some examples are shown for such materials as: Cu, Al, Zn, Fe, Ti, Mo, W, and Al_2O_3. Various practical aspects of the obtained results are discussed, with a special attention given to less or no intuitively predictable dependencies.

Key words computer simulation • heat flow • thermal evolution

W. Szymczyk✉, Z. Werner
Department of Materials Modification,
The Andrzej Soltan Institute for Nuclear Studies,
05-400 Otwock-Swierk, Poland,
Tel: +48 22/ 718 05 62, Fax: +48 22/ 779 34 81,
e-mail: szymczyk@ipj.gov.pl

J. Piekoszewski
Department of Nuclear Methods of Material Engineering,
Institute of Nuclear Chemistry and Technology,
16 Dorodna Str., 03-195 Warsaw, Poland
and Department of Materials Modification,
The Andrzej Soltan Institute for Nuclear Studies,
05-400 Otwock-Swierk, Poland

W. Szyszko
Department of Ion Physics and Implantation,
Institute of Physics,
Maria Curie-Skłodowska University,
1 M. Curie-Skłodowskiej Sq., 20-031 Lublin, Poland

Received: 8 August 2001, Accepted: 17 May 2002

Introduction

Over the past two decades several groups all over the world investigated applications of high intensity pulsed ion and plasma beams (HIPIPB) to surface treatment of materials [1, 3, 5–7]. The HIPIPB techniques combine some features of laser treatment and ion implantation, since both heat and mass transfer occurs in the "beam-target" system. Beam parameters vary widely depending on the kind of application. Ion energy may range from few keV to 1 MeV, pulse duration from 10 ns to 10 ms, energy density from 0.01 to 50 J/cm^2. The most characteristic feature of the HIPIPB technique is that pulse irradiation melts the near-surface layer of target material in a time scale from ns to ms. The ultimate properties of the processed materials depend on the kind of material itself, kind of ions in the beam and heat evolution in the substrate. In the literature published thus far there exist a lot of reports dealing with dynamics of the processes induced by pulsed laser or electron irradiation of solids. However, consideration of thermal processes induced by HIPIPB are rather sparse.

The aim of this paper is to get insight into heat evolution within targets of various materials irradiated with plasma beams of diameters in the range of several centimeters, Gaussian-shaped pulses of duration τ_p between 0.1 and 3 μs full width at half magnitude (FWHM), and depositing on the target surfaces energy densities E in the range 1–10 J/cm^2. These beam parameters are typical for pulses generated in the rod plasma injector and magnetically insulated high voltage diode types of facilities, which are most frequently used in material treatment experiments.

Method of calculation

When energy is delivered to regions of lateral dimensions (y,z) much greater than the heat diffusion length in material bulk (which is the case in our experiments) and convection currents can be ignored, one-dimensional diffusion equation may be used to calculate thermal evolution [9]:

$$(1) \quad C_s(T)\rho(T)\frac{\partial T(x,t)}{\partial t} = \frac{\partial}{\partial x}\left[K(T)\cdot\frac{\partial T(x,t)}{\partial x}\right] + G(x,t)$$

where $T(x,t)$ is temperature distribution at the depth x and time t within the irradiated target, $C_s(T)$ is the target material specific heat, $\rho(T)$ is the target material density, and $K(T)$ is the target material heat conductivity. The source term $G(x,t)$ is proportional to the energy absorbed within the target surface layer; it is given by $Q_{ab}(\Delta x,t) \sim Q_{pulse}(t)$ where $Q_{pulse}(t)$ is the beam pulse energy. The energy loss due to the Planck radiation, surface evaporation and heat convected to the surroundings are very small compared to the beam energy and, therefore, are not included into the source term.

Heat convection equation can be solved analytically or numerically. An analytical solution is almost impossible in the case of multi-layer systems, in which phase transitions take place and thermal parameters are temperature-dependent. In this paper the Finite Element Method [4, 8] was used to determine the $T(x,t)$ temperature evolution numerically. The ETLIT program (Energy Transport in Laser Irradiated Targets) was modified and adopted to calculations of heat transport in multi-component targets (up to 5 different materials in any configuration) irradiated by pulsed plasma beams. Phase transition, e.g. melting and solidification and temperature--dependent thermal properties of the samples were taken into account. Fixed-grid approach for tracing the moving phase boundary was used.

In the present calculations 1000 μm thick targets were divided into smaller regions (elements). Constant element thickness Δx=0.01 μm was chosen in the vicinity of the target surface. To avoid excessive calculation time and to save computer memory, progressively longer distances between deeper nodes were adopted. The energy pulse was divided into small Δt_i intervals, usually 0.05–0.1 μs. It was assumed that the whole target volume initially was at the ambient temperature, i.e. $T(x,t=0)=T_0$, where T_0 is the ambient temperature.

The m boundary condition must be specified at each boundary point in case of a differential equation of order $2m$. In our simulations two edge conditions were necessary. The first condition is that the energy flux absorbed at the surface is totally converted into heat. If $\tau(t_i)$ is the mean energy flux during the time interval Δt_i, and $Q_{ab}(\Delta x_1,t_i)$ is heat absorbed within the surface layer Δx_1 during time interval Δt_i, then the condition may be written down as:

$$(2) \quad Q_{ab}(\Delta x_1 t_i) \sim \tau(t_i)\Delta t_i$$

The second boundary condition is that temperature at the back--side of the target is close to the ambient temperature T_0 at all times:

$$(3) \quad T(x_{max}, t_i) = T_0$$

A linear temperature dependence within each element and perfect thermal contact between adjacent layers were assumed.

The $\tau(t_i)$ pulse may have an arbitrary shape e.g. Gaussian form, rectangle, series of rectangles, series of triangles etc. In the present calculations the pulses were assumed to be of Gaussian form with different widths and amplitudes.

Under energy deposition the temperature of any given ith element within the target rises up until it reaches the melting point T_m, which occurs at the time of melting $t_{melting}$. Subsequent energy deposited within that element is accumulated until the value $\Delta E_i = H_i * m_i$ corresponding to the latent heat of melting that element is reached (H_i and m_i are latent heat and mass of the ith element, respectively). Thermodynamical parameters for liquid phase of the material involved are used for the period the layer remains molten. Solidification is taken into account in a similar manner: when a molten layer cools down, its temperature falls down to the solidification point and remains constant until the ΔE_i energy accumulated within the ith element dissipates. End of melting ($t_{solidification}$) is determined as the moment at which solidification of the ith layer is finished. The melt duration is defined as $t_L = t_{solidification} - t_{melting}$.

The calculation results are returned in a two-dimensional matrix, which contains data necessary to determine temperature profile within the target after each time interval Δt_i, the temperature on time dependency in each target node x_i, the melt duration, and the maximum melt depth.

In the present calculations the above mentioned (K, C_s, ρ) and other necessary material data (e.g. melt temperature) have been taken after [2] and [10]. In case no data could be found in literature for the liquid phase temperature region, the solid state values for temperatures close to the melt temperature have been taken. According to the recent data found in [11], the density of alumina in liquid state is by 27% lower than that in solid state. We checked that even for the alumina case, taking equal values of density for both states results in the maximum melt depth higher only by 8.3% in comparison to the depth obtained when the true liquid state density value is taken; melt duration practically does not change at all. Density of metals does not change so much as density of alumina, therefore we consider that for rough estimations there is no need to take into account the difference between solid and liquid state densities.

Results and discussion

In order to get insight into heat evolution in materials with thermal properties spanning over a wide range of values, for the first round of calculations we selected 3 materials of very different melting temperatures and heat conductivities: copper, iron and alumina (melting point increases and heat conductivity decreases for successive materials in this group). Melt depth d_M *vs.* pulse energy density E dependencies at irradiation with Gaussian pulses of FWHM=0.1, 1.0 and 3.0 μs for the three studied materials are shown in Fig. 1. The following qualitative trends can be noticed:

(a) both the energy density thresholds for melting E_M and their ranges for 0.1, 1.0 and 3.0 μs pulses decrease in the Cu → Fe → Al_2O_3 sequence;
(b) melt depth *vs*. energy curves for different pulse durations converge with increasing energy, and the energy density E_{CM} at which the convergence occurs also decreases in the Cu → Fe → Al_2O_3 sequence;
(c) slope of the melt depth *vs*. pulse energy curve also decreases in the above sequence of materials.

Qualitatively, the trend observed in (a) is understandable in view of the fact that for a given power density dissipated at

the surface, heat accumulation in this region is more effective for a material with lower heat conductivity – which coincides with the Cu →Fe→ Al_2O_3 sequence. Convergence of d_M versus E curves for various pulse durations i.e. trend (b) can be accounted for by the time of heat diffusion t_D required to travel over the molten region and to reach the liquid-solid interface. If t_D is sufficiently longer than the pulse duration – which occurs at large E and thereby long t_D – then the d_M versus E dependence becomes insensitive on the pulse duration. Decrease of E_{CM} with lowering heat conductivity is simply due to an increase of t_D as it is the case in the Cu→Fe→Al_2O_3 sequence.

Figure 2 shows dependencies of the melt duration t_L on energy density E for the same pulse widths and materials as in Fig. 1. The following main qualitative trends can be inferred from that figure:

(d) melt duration t_L increases at a given energy density in the Cu → Fe → Al_2O_3 sequence;
(e) melt duration t_L *vs*. energy E curves for different pulse durations converge for higher densities of irradiation energy, and the energy density E_{CL} at which the convergence occurs decreases also in the Cu→Fe→Al_2O_3 sequence;
(f) $t_L=f(E)$ curves in the energy range $E_M<E<E_{CL}$ differ in shape and numerical values for 0.1, 1.0 and 3.0 μs pulses for all materials Cu, Fe and Al_2O_3; the slopes $\Delta t_L/\Delta E$ being always greater for longer pulses.

Observation (d) is rather self-explanatory considering the fact that the poorer heat transport from liquid-solid interface owing to lower heat conductivity, the longer time to solidification. Convergence of the $t=f(E)$ curves mentioned in (e) can be readily understood by considering relation between the pulse duration and the liquid duration t_L. If material remains in the liquid phase sufficiently long after the irradiating energy pulse has ceased, melt duration $t_L=f(E)$ should not depend on the pulse duration. Therefore, in an example shown in Fig. 2, almost perfect convergence is seen for liquid durations longer than the longest pulse width 3 μs used in these calculations. At the moment, the observation (f) is for us beyond the intuitive reach, since melting point, heat conductivity, and heat capacity values influence the heat evolution in quite a complicated way. However, some important practical hints can be derived from the example shown in Fig. 2.

It is obvious that processing time in the pulsed-beam techniques is too short to allow for any real-time control. Moreover, plasma, ion, as well as laser or electron pulses have a finite reproducibility. Therefore, if one wishes to carry out a process in which liquid duration should be relatively short (say below 2 μs) – i.e. at an energy density below E_{CL} – then a short irradiation pulse is clearly desirable. In such case a given fluctuation in energy density causes only a small variation in liquid duration. In case of long pulses the reverse is true. On the other hand, if liquid duration has to be long and hence the energy density must exceed E_{CL}, then wider pulses are desirable: effects of surface deterioration are less probable at lower power densities.

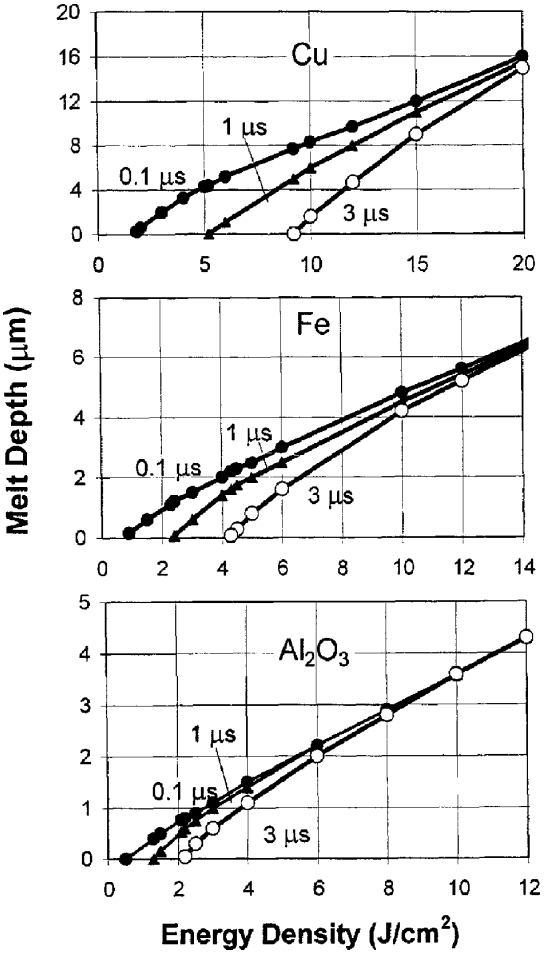

Fig. 1. Melt depth *vs*. energy density for Gaussian plasma pulses of 0.1, 1, and 3 μs FWHM width in Cu, Fe, and Al_2O_3 targets.

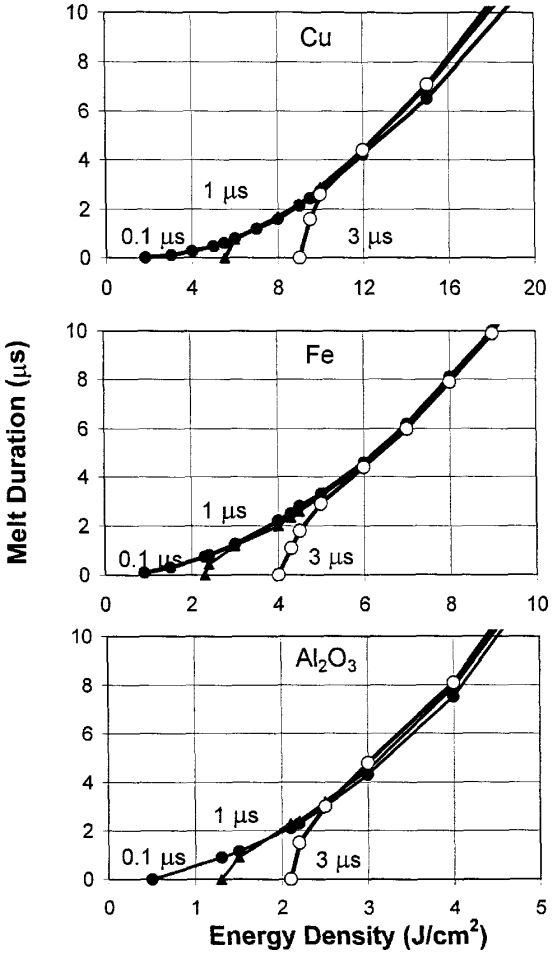

Fig. 2. Melt duration *vs*. energy density for Gaussian plasma pulses of 0.1, 1, and 3 μs FWHM width in Cu, Fe, and Al_2O_3 targets.

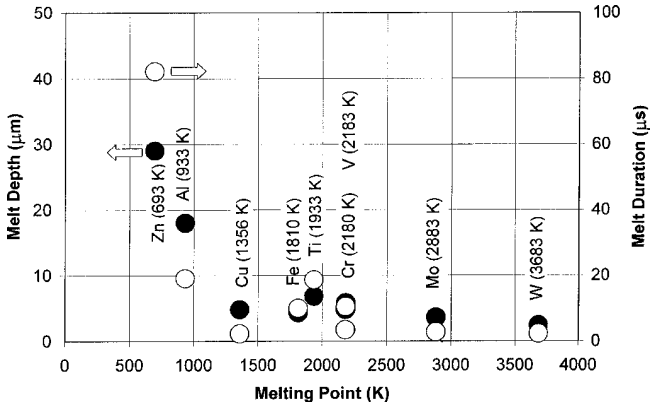

Fig. 3. Melt depth and melt duration *vs*. melting point for various elements. Data calculated assuming irradiation with Gaussian plasma pulses of energy density 10 J/cm^2 and 1 μs FWHM width.

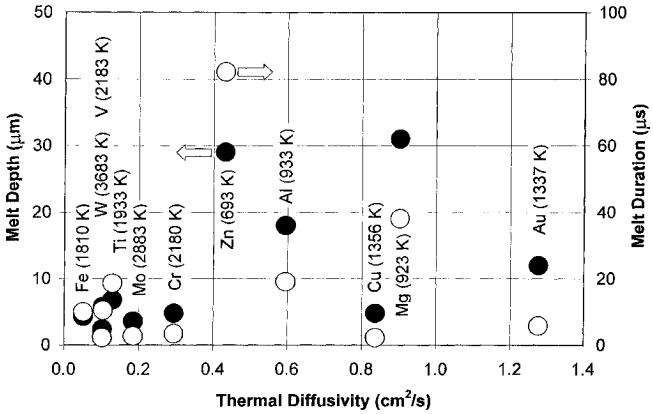

Fig. 4. Melt depth and melt duration *vs*. thermal diffusivity of various elements. Data calculated assuming irradiation with Gaussian plasma pulses of energy density 10 J/cm^2 and 1 μs FWHM width.

Another practical information can be derived from Fig. 3 in which melting depths and liquid durations are compiled for various elements covering a wide range of melting points T_M. We have used pulses of 1 μs width and E=10 J/cm^2 to calculate these data. An unexpected result is that both melt depth d_M and melt duration t_L depend significantly on T_M only for relatively low melting points (for Zn and Al in our data set). For all materials starting from copper (T_M=1356K for Cu) till tungsten (T_M=3683K for W) both d_M and t_L values stay within a narrow window (below 10 and 20 μs, respectively) – without any clear dependence on the melting point. The same regularity are observed for shorter pulses (0.1 μs), although the absolute values of melt depth d_M are slightly higher. For longer pulses (10 μs) many of the materials selected for calculations do not melt at all. However, to our knowledge such long pulses are not used in practice.

In Fig. 4 we plotted the d_M and t_L values calculated as above versus thermal diffusivity $D_T=(K/\rho\times C_s)^{1/2}$. Abscissa values of the data points were calculated assuming constant K and C_s values corresponding to the near-melting point; however, ordinate values were calculated with $K(T)$ and $C_s(T)$ dependencies taken into account. The assumption is justified by the generally weak dependencies of these parameters on temperature – at least for metals, as opposite for e.g. silicon. As can be seen, for diffusivities D_T below 0.2 cm^2/s the values of d_M and t_L stay below 10 μm and 20 μs, respectively. Unfortunately, for D_T >0.3 cm^2/s no regularity is observed.

Conclusions

Results of computer simulation of thermal evolution occurring in various targets irradiated with high intensity pulsed ion or plasma beams of wide range of energy densities and pulse duration can be summarized as follows.

- Both energy density thresholds for melting E_M and their ranges for pulses of 0.1, 1.0 and 3.0 μs duration decrease with increasing melting point and decreasing thermal conductivity as it has been demonstrated for the Cu → Fe → Al_2O_3 sequence.
- Families of the melt depth and the melt duration *vs*. energy curves, plotted for different pulse duration as a parameter, converge with increasing energy. Energy densities at which the convergence occurs, decreases also in the Cu→Fe→Al_2O_3 sequence. Slope of the melt depth *vs*. energy density curve also decreases in the above sequence of materials.
- For energies between the melting threshold and convergence point, the melt duration on energy density curves differ significantly in shape and in numerical values for different values of pulse durations (FWHM=0.1, 1.0 and 3.0 μs), and for different materials (Cu, Fe, and Al_2O_3). Slope of these curves is always greater for longer pulses.

It is believed that analysis of the graphs shown in this work may facilitate the choice of beam parameters for processing different materials by the HIPIPB technique.

References

1. Biller W, Heyden D, Müller D, Wolf GK (1999) Modification of steel and aluminum by pulsed energetic ion beams. Surf Coat Tech 116:537–542
2. Data compendium for plasma-surface interactions (1984) Nuclear Fusion, Special Issue. IAEA, Vienna
3. Gyulai J, Krafcik I (1989) Comparative status of pulsed ion implantation. Nucl Instrum Meth B 37/38:275–281
4. Hughes TJR (ed) (1987) The Finite Element Methods – Linear Statistic and Dynamic Finite Element Analysis. Prentice-Hall, Englewood Cliffs, New York
5. Piekoszewski J, Langner J (1991) High intensity pulsed ion beams in material processing: equipment and applications. Nucl Instrum Meth B 53:148–153
6. Pogrebnjak AD, Remnev GE, Kurokin IB, Ligachev AE (1989) Structural, physical and chemical changes induced in metals and alloys exposed to high power ion beams. Nucl Instrum Meth B 36:286–292
7. Rej DJ, Davis HA, Olson JC (1997) Materials processing with intense pulsed ion beams. J Vac Sci Technol A 15;3:1089–1093
8. Ruan Y, Zabaras N (1991) An inverse finite element technique to determine the change of phase interface location in two-dimensional melting problems. Commun Appl Numer Meth 7:325–338
9. Szyszko W, Vega F, Afonso CN (1995) Shifting of the thermal properties of amorphous germanium films upon relaxation and crystallization. Appl Phys A 61:141–147
10. Touloukian ES (ed) (1970) Thermophysical properties of matter. Vol. 1: Thermal conductivity – metallic element and alloys. IFI/Plenum Press, New York
11. University of Aberystwyth, Department of Physics (2001) Annual Report 2000